High-throughput computation and machine learning of refractive index of polymers ⊘

Special Collection: Accelerate Materials Discovery and Phenomena

Ankit Mishra ; Pankaj Rajak ; Ayu Irie; Shogo Fukushima ; Rajiv K. Kalia; Aiichiro Nakano ✉ ; Ken-ichi Nomura ; Fuyuki Shimojo ; Priya Vashishta

Check for updates

View Online

Export Citation

CrossMark

Articles You May Be Interested In

Photon management with superlattice for image sensor pixels

AIP Advances (August 2021)

High-throughput computation and machine learning of refractive index of polymers

View Online   Export Citation   CrossMark

Ankit Mishra,[1] (iD) Pankaj Rajak,[1] (iD) Ayu Irie,[1,2] Shogo Fukushima,[3] (iD) Rajiv K. Kalia,[1] Aiichiro Nakano,[1,a)] (iD)
Ken-ichi Nomura,[1] (iD) Fuyuki Shimojo,[2] (iD) and Priya Vashishta[1] (iD)

AFFILIATIONS

[1]Collaboratory for Advanced Computing and Simulations, University of Southern California, Los Angeles,
California 90089-0242, USA
[2]Department of Physics, Kumamoto University, Kumamoto 860-8555, Japan
[3]Institute for Materials Research, Tohoku University, Sendai 980-8577, Japan

Note: This paper is part of the APL Special Collection on Accelerate Materials Discovery and Phenomena.
[a)]Author to whom correspondence should be addressed: anakano@usc.edu

ABSTRACT

Refractive index (RI) of polymers plays a crucial role in the design of optoelectronic devices, including displays and image sensors. We have developed a framework for (1) high-throughput computation of RI values for computationally synthesized amorphous polymer structures based on a generalized polarizable reactive force-field (ReaxPQ+) model, which is orders-of-magnitude faster than quantum-mechanical methods; (2) prediction of composition–structure–RI relationships based on a machine-learning model based on graph attention neural network; and (3) computation of frequency-dependent RI combining ReaxPQ+ and Lorentz-oscillator models. The framework has been tested on a computational database of amorphous polymers.

Refractive index (RI) is a fundamental material constant that governs propagation of light in an optical medium, thus serving as a key material design parameter for optical applications.[1] Polymers constitute essential components of many advanced optoelectronic devices, including displays and image sensors.[2–7] The attractiveness of polymers in these applications lies not only in their easy processability into various forms, mechanical flexibility, and low cost of fabrication but also in fine tunability of RI values through chemical modifications. Further developments of advanced polymers for high-performance optical applications would be greatly accelerated by high-throughput computational screening of polymers with desired RI values as well as machine learning (ML) of composition–structure–RI relationships. Despite tremendous advances in materials genome (i.e., applying informatics to design new materials significantly faster than the conventional trial-and-error approach),[8,9] high-throughput RI computation of polymers remains elusive. This is mainly due to high computational costs of quantum-mechanically evaluating RI[10] for large system sizes required to account for complex chemical and morphological features (e.g., crystalline vs amorphous) that dictate optical responses of polymers.

In this paper, we address the high-throughput RI-computation challenge through recent developments in first principles-informed reactive molecular dynamics (RMD) simulations[11,12] based on a generalized polarizable reactive force-field (ReaxPQ+) model.[13] The original ReaxPQ model used a polarizable charge equilibration (PQEq) scheme to describe electronic polarization.[14,15] The ReaxPQ+ model further incorporates the effect of external electric field to accurately calculate RI in orders-of-magnitude shorter computational time compared to quantum-mechanical (QM) methods.[13] Using ReaxPQ+, we construct a large computational dataset of amorphous polymers (Fig. 1) and thereby train a ML model based on graph attention neural network.[16] We further combine ReaxPQ+ with a simple Lorentz-oscillator model to calculate frequency-dependent RI.[17]

We first compute RI using polarizable charge equilibration scheme. In the original reactive force-field (ReaxFF) model for RMD simulations, the potential energy, $E(\{\mathbf{r}_i | i = 1, \ldots, N\}, \{q_i | i = 1, \ldots, N\})$, is composed of bonding (E_b) and nonbonding (E_{nb}) terms, where $\mathbf{r}_i$ and q_i are the position and charge of the ith atom (N is the number of atoms).[11,12] E_b describes the formation and breakage of chemical bonds through reactive bond orders, BO_{ij}, between atomic pairs, (i, j). E_{nb} is composed of van der Waals (E_{vdW}) and Coulombic ($E_{Coulomb}$) terms. Interatomic charge transfer is described by a charge equilibration (QEq) scheme, in which $E_{Coulomb}$ is minimized as a
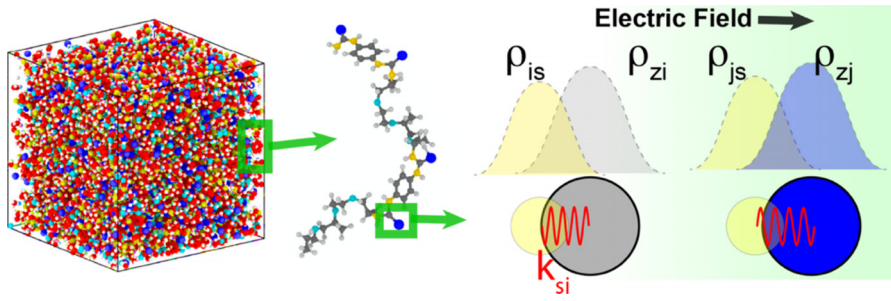
function of atomic charges subject to the charge neutrality condition, $\sum_i q_i = 0$.[18,19] A breakthrough in computationally efficient description of electronic polarization was achieved by an extension of ReaxFF, i.e., PQEq-based ReaxPQ+.[13] In the PQEq scheme, electric polarization is described using a Gaussian-shaped electron density (shell) that can polarize away from the nuclei core in response to both external electric fields and internal electric fields produced by other atoms. Here, each atom i is partitioned into two charged sites (i.e., core and shell). The core (ρ_{ic}) consists of two parts: (1) ρ_i with a variable total charge (q_i); and (2) ρ_{Zi} with a fixed total charge (Z_i). The massless shell (ρ_{is}) has a fixed total charge of $-Z_i$. The shell and core of an atom are connected by an isotropic harmonic spring with an element-specific force constant K_{si} (Fig. 1). The resulting $E_{Coulomb}$ involves core–core, core–shell, shell–core, and shell–shell interactions,

$$
\begin{aligned}
E_{\text{Coulomb}}(\{\mathbf{r}_{ic}, \mathbf{r}_{is}, q_i\}) = \sum_{i=1}^{N} &\left[\chi_i^0 q_i + \frac{1}{2} J_{ii}^0 q_i^2 + \frac{1}{2} K_{si} r_{ic,is}^2 \right] \\
+ \sum_{i>j} &\left[T(r_{ic,jc}) C_{ic,jc}(r_{ic,jc}) q_{ic} q_{jc} \right. \\
&- T(r_{ic,js}) C_{ic,js}(r_{ic,js}) q_{ic} Z_j \\
&- T(r_{is,jc}) C_{is,jc}(r_{is,jc}) Z_i q_{jc} \\
&\left. + T(r_{is,js}) C_{is,js}(r_{is,js}) Z_i Z_j \right],
\end{aligned} \tag{1}
$$

where $\mathbf{r}_{ic}$, $\mathbf{r}_{is}$, χ_i^0, and J_{ii}^0 are the core position, shell position, electronegativity, and hardness of the ith atom. In Eq. (1), $r_{ia,jb}$ ($i, j = 1, \ldots, N$; $a, b = c$—core or s—shell) are charge–charge distances. The electrostatic energy between two Gaussian charges is given in terms of the error function $C_{ia,jb}(r_{ia,jb})$, and the Coulombic interaction is screened using a taper function $T(r)$. The core–core, core–shell, shell–core and shell–shell charge interactions in Eq. (1) has quadrupled charge computation over the conventional ReaxFF model, which has been accelerated through a series of computational transformations,[13] including extended Lagrangian-based shadow dynamics.[20,21]

To compute the RI of each amorphous polymer structure, we apply an external electric field, $\mathcal{E}$, and relax the shell positions, $\{\mathbf{r}_{is}\}$, to the minimum-energy configuration.[13] We then calculate the induced polarization as

$$
\Delta \mathbf{P}_{\mathcal{E}} = \sum_{i=1}^{N} \sum_{a \in \{c,s\}} q_{ia}(\mathbf{r}_{ia} - \mathbf{r}_{ia}^0), \tag{2}
$$

where q_{ia} and $\mathbf{r}_{ia}^0$ are charges and their positions in the absence of external electric field. RI is then obtained as

$$
n = \sqrt{1 + 4\pi \frac{\Delta P_{\varepsilon}}{\varepsilon}}, \tag{3}
$$

where $\Delta P_{\varepsilon}/\varepsilon$ denotes the average of the diagonal elements of the dielectric tensor, $\Delta \mathbf{P}_{\varepsilon}/\varepsilon$.

We next predict composition–structure–RI relationships using graph attention neural network (GAT). We consider a graph, $G = (V, E)$, where V is the set of atoms (or nodes) and E is the set of bonds between atomic pairs (or edges); see Fig. 2(a). A graph neural network computes the embedding for each node by aggregating neighborhood information from adjacent nodes, which involves two essential steps of message passing and message aggregation [Fig. 2(b)].[16] This step is propagated through multiple layers. At lth layer, each node aggregates information about other nodes that are l-hops away from it. Given an initial feature X_v of each node v, GAT learns the final feature Z_v by recursively computing the embedding, $h_v^{(l)}$, of the vth node at layer l,

$$
h_v^{(0)} = X_v, \tag{4}
$$

$$
h_v^{(l)} = \sigma\left(\sum_{u \in N(v)} \alpha_{vu} W^{(l)} h_u^{(l-1)} \right), \quad l \in \{1, \ldots, L\}, \tag{5}
$$

$$
Z_v = h_v^{(L)}. \tag{6}
$$
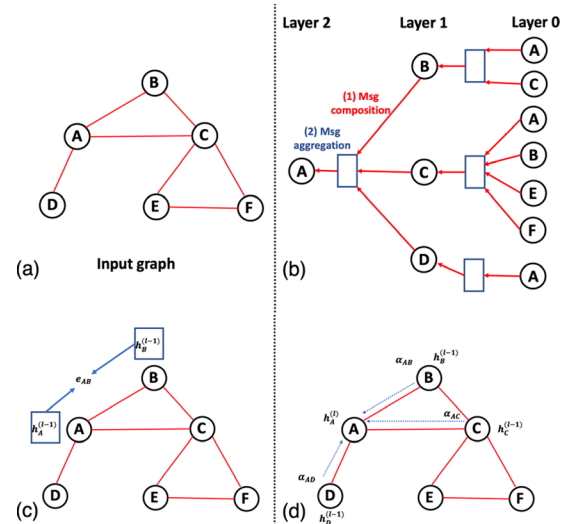

FIG. 2. (a) An example graph, where the nodes are labeled by alphabet letters and the edges are represented by red lines. (b) Layers of message composition and aggregation operations on the sample graph in graph neural network. (c) Computation of attention coefficients e_{vu} in graph attention neural network; see Eq. (8). (d) Computation of weighting factors α_{vu} in Eq. (7).

Here, $N(v)$ is the set of adjacent nodes of node v, and L is the last layer. In Eq. (5), the message $m_u^{(l)} = W^{(l)} h_u^{(l-1)}$ transforms neighbor u's embedding in the previous layer using learnable parameter $W^{(l)}$. Messages from all adjacent nodes are summed with a weighting factor,

$$\alpha_{vu} = \frac{\exp(e_{vu})}{\sum\limits_{k \in N(v)} \exp(e_{vk})}, \qquad (7)$$

i.e., a softmax function applied to attention coefficients,

$$e_{vu} = a\left(W^{(l)} h_u^{(l-1)}, \ W^{(l)} h_v^{(l-1)}\right), \qquad (8)$$

where the attention mechanism a is a simple neural network of single-layer depth; see Figs. 2(c) and 2(d).[22] We improve the attention coefficients using multi-head attention computation, which generates an ensemble of attention scores with a different set of parameters. This is followed by application of a nonlinear rectified linear unit (ReLU), σ, to produce the embedding at layer l as shown in Eq. (5).

To compute frequency-dependent RI of polymers, we further developed a simple Lorentz-oscillator model,[17] taking advantage of the unique polarizable feature of the ReaxPQ+ model while augmenting its massless shells[13] to describe dynamics. Frequency-dependent RI based on an extended Lorentz model is expressed as

$$n(\omega) = \sqrt{\left| 1 - \sum_{i=1}^{N_{\text{element}}} \frac{4\pi e_i^{*2} n_i}{m_i^* \omega^2 - K_{si}} \right|} \quad (\omega < \min_i(\omega_i)), \qquad (9)$$

where ω is the frequency, N_{element} is the number of elements (C, H, etc.), n_i and K_{si} are the number density of atoms and spring constant for the ith element in the atomic unit, and ($\omega_i = \sqrt{K_{si}}$). Here, effective mass m_i^* (in unit of the electron mass) and effective charge e_i^* (in unit of the electron charge) are introduced to account for many-body screening. Note that Eq. (9) is valid below the resonant frequencies, ω_i, of constituent elements.

In the baseline model, we adopt K_{si} values that have been computed based on the PQEq method within the ReaxPQ+ model,[13] whereas $e_i^* = m_i^* = 1$ for all elements. For a given material system, for which the static $n = n(0)$ has been computed using RMD simulation based on the ReaxPQ+ model, e_i^* of all the elements are uniformly scaled to reproduce the ReaxPQ+ value as

$$e_i^* = \sqrt{\frac{n(0)_{\text{ReaxPQ+}}^2 - 1}{n(0)_{\text{baseline}}^2 - 1}}. \qquad (10)$$

This incorporates the many-body screening effect in RMD simulations, which is absent in the Lorentz-oscillator model. Furthermore, m_i^* values can be adjusted if one would like to reproduce $n(\omega)$ values computed using, e.g., first-principles QM calculation for a particular frequency; see the supplementary material for more details on methods.

We have incorporated the ReaxPQ+ model into our high-throughput computational synthesis framework of amorphous polymer structures.[23] We have thereby constructed a large dataset of structurally diverse 1276 polymers with quantum accuracy for a class of flexible all-organic polyolefins composed of C, H, O, N, S, F, Cl, and Br; for details, see Refs. 23 and 24. In this work, we apply the new RI computation methods to these datasets.
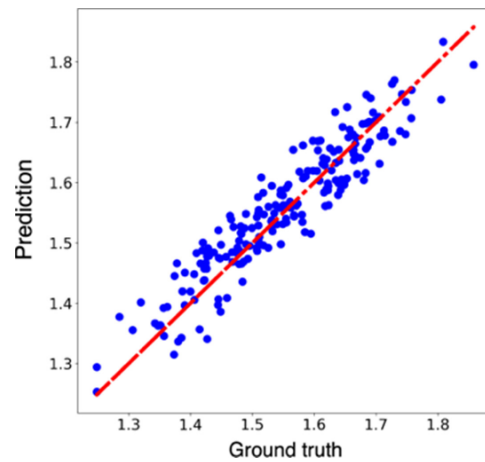

FIG. 3. Graph attention neural network model prediction vs ground-truth ReaxPQ+ values of refraction index. Correlation coefficient is 0.89.

The initial feature, X_v in Eq. (4), is a 12-dimensional vector composed of Pauling electronegativity, electron affinity, group in periodic table, covalent radius, ionization energy, number of s electrons, number of p electrons, atomic polarizability, ionization affinity ratio, liquid range, liquid ratio, and ratio of electron affinity to electronegativity. Total number of network parameters is 62 017. The network is trained for 100 epochs, where the training and test root mean square errors (RMSE) drop to 0.10 within the first 20 epochs. Figure 3 compares GAT model predictions with ground-truth ReaxPQ+ values.

The attention mechanism in GAT allows us to visualize local features that are relevant for RI. Figure 4(a) shows a monomer of one of the polymers in the computational dataset, where the color represents the local features learned by GAT, which reveals the importance of CF_3 group [see the three fluorine atoms colored red, which are connected to the carbon atom colored dark red at the bottom of Fig. 4(a)]. Inspired by this finding, we have compared a subset of polymers in the dataset, for which the number of fluorine-containing groups in eight-chain polymer varies. Figure 4(b) indeed shows clear correlation between RI value and fluorine content.

We have further used the PQEq-Lorentz model to compute frequency-dependent RI. To demonstrate the optional use of m_i^*
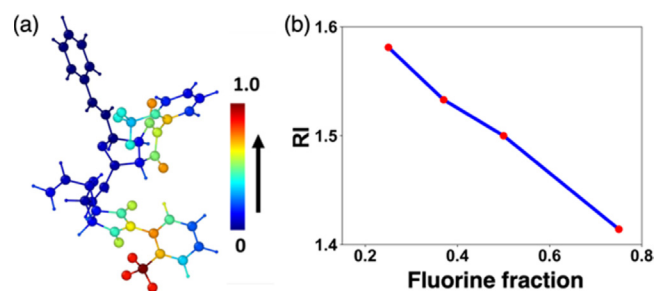

FIG. 4. (a) Visualization of local features that correlate with RI value. (b) RI value as a function of fluorine content.
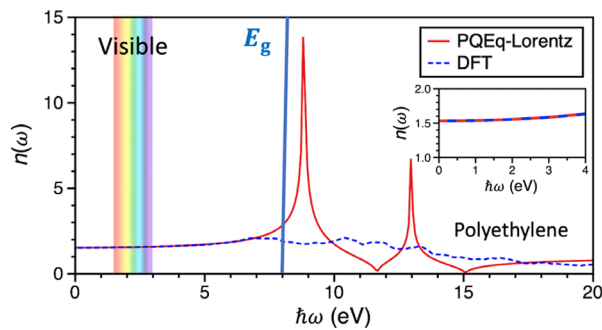
08 October 2023 17:43:35

FIG. 5. Frequency-dependent refractive index of polyethylene computed using the PQEq-Lorentz model (solid red line) and first-principles DFT calculation (dashed blue line). Bandgap, E_g, is indicated by solid cyan line, whereas the visible spectral range of interest is marked by a rainbow stripe. The inset magnifies the visible spectral range.

parameters, we here use *ab initio* density functional theory (DFT) calculation of $n(\omega)$ for polyethylene (PE) using the QXMD code.[25] The electronic states are calculated using projector augmented wave (PAW) method.[26,27] Projector functions are generated for the $2s$ and $2p$ states of C and the $1s$ state of H. The generalized gradient approximation (GGA) is used for the exchange-correlation energy.[28] The momentum-space formalism is utilized, where the plane wave cutoff energies are 30 and 250 Ry for the electronic pseudo-wave functions and pseudo-charge density, respectively. The Γ point is used for Brillouin zone sampling for electronic-structure calculations. The van der Waals interaction between atoms is described in the DFT-D approach.[29] The system is composed of $2 \times 3 \times 4$ PE crystalline unit cells in an orthorhombic simulation box of size $14.8 \times 14.8 \times 10.136$ Å^3. Figure 5 shows good agreement between the Lorentz model and DFT calculation below the calculated bandgap, $E_g \sim 8$ eV, only to which the Lorentz model applies. Especially, the two calculations are indistinguishable in the visible spectral range of interest.

In summary, we have developed a framework for high-throughput computation of refraction index and its frequency dependence based on a generalized polarizable reactive force-field (ReaxPQ+) model, which is orders-of-magnitude faster than quantum-mechanical methods, as well as prediction of the composition–structure–RI relationships based on graph attention neural network. While the framework may readily find applications in rational design of advanced polymers for high-performance optical applications, the graph network could potentially be improved by group-theoretical equivariance for accuracy[30] and sharpness-aware minimization for robustness.[31]

See the supplementary material for details of the model accuracy and the computational efficiency comparisons between this study and other methods along with experimental validations for ML and ReaxPQ+ calculations.

AUTHOR DECLARATIONS

Conflict of Interest

The authors have no conflicts to disclose.

Author Contributions

Ankit Mishra: Data curation (equal); Investigation (equal); Methodology (equal); Writing – original draft (equal). **Pankaj Rajak:** Methodology (equal); Software (equal); Writing – review & editing (equal). **Ayu Irie:** Investigation (equal); Validation (equal); Writing – review & editing (equal). **Shogo Fukushima:** Investigation (equal); Validation (equal); Writing – review & editing (equal). **Rajiv K. Kalia:** Conceptualization (equal); Supervision (equal); Writing – review & editing (equal). **Aiichiro Nakano:** Conceptualization (equal); Funding acquisition (equal); Methodology (equal); Supervision (equal); Writing – original draft (equal). **Ken-ichi Nomura:** Conceptualization (equal); Methodology (equal); Supervision (equal); Writing – original draft (equal). **Fuyuki Shimojo:** Methodology (equal); Supervision (equal); Writing – review & editing (equal). **Priya Vashishta:** Conceptualization (equal); Resources (equal); Supervision (equal); Writing – review & editing (equal).

DATA AVAILABILITY

The data that support the findings of this study are available from the corresponding author upon reasonable request.

REFERENCES

[1]D. R. Smith, J. B. Pendry, and M. C. K. Wiltshire, Science **305**(5685), 788–792 (2004).
[2]T. Higashihara and M. Ueda, Macromol **48**(7), 1915–1929 (2015).
[3]D. H. Kim, W. Jang, K. Choi, J. S. Choi, J. Pyun, J. Lim, K. Char, and S. G. Im, Sci. Adv. **6**(28), eabb5320 (2020).
[4]I. Oshiyama, T. Shigetoshi, I. Mita, N. Sumitani, T. Oinoue, S. Saito, T. Okawa, Y. Ebiko, Y. Yokochi, Y. Kitano, Y. Hagimoto, T. Hirano, and H. Iwamoto, in Proceedings of the EDTM, 2021.
[5]M. Briesenick, M. Gallei, and G. Kickelbick, Macromol **55**(11), 4675–4691 (2022).
[6]K. Mazumder, H. Komber, E. Bittrich, B. Voit, and S. Banerjee, Macromol **55**(3), 1015–1029 (2022).
[7]C. Pina-Hernandez, K. Yamada, A. Legacy, and K. Munechika, Proc. SPIE **12449**, 1244905 (2023).
[8]A. Jain, K. A. Persson, and G. Ceder, APL Mater. **4**(5), 053102 (2016).
[9]C. Kim, A. Chandrasekaran, T. D. Huan, D. Das, and R. Ramprasad, J. Phys. Chem. C **122**(31), 17575–17585 (2018).
[10]Y. Zhang, C. Wang, F. Zheng, and P. Zhang, Phys. Rev. E **86**(6), 061111 (2012).
[11]A. C. T. van Duin, S. Dasgupta, F. Lorant, and W. A. Goddard, J. Phys. Chem. A **105**(41), 9396–9409 (2001).
[12]K. Nomura, R. K. Kalia, A. Nakano, P. Vashishta, A. C. T. van Duin, and W. A. Goddard, Phys. Rev. Lett. **99**(14), 148303 (2007).
[13]K. Liu, S. Hong, R. K. Kalia, A. Nakano, K. Nomura, P. Rajak, S. Tiwari, P. Vashishta, Y. Luo, N. A. Romero, S. S. Naserifar, W. A. Goddard, and M. Kunaseth, in Proceedings of the ScalA18 (IEEE, 2018), pp. 41–48.
[14]S. Naserifar, D. J. Brooks, W. A. Goddard, and V. Cvicek, J. Chem. Phys. **146**(12), 124117 (2017).
[15]Y. Li, K. Nomura, J. Insley, V. Morozov, K. Kumaran, N. A. Romero, W. A. Goddard III, R. K. Kalia, A. Nakano, and P. Vashishta, Comput. Sci. Eng. **21**(5), 64–75 (2019).
[16]Z. Wu, S. Pan, F. Chen, G. Long, C. Zhang, and P. S. Yu, IEEE Trans. Neural Networks Learn. Syst. **32**(1), 4–24 (2021).
[17]A. B. Djurisic and E. H. Li, Appl. Opt. **37**(22), 5291–5297 (1998).
[18]A. K. Rappe and W. A. Goddard, J. Phys. Chem. **95**(8), 3358–3363 (1991).
[19]A. Nakano, Comput. Phys. Commun. **104**(1–3), 59–69 (1997).

[20]K. Nomura, P. E. Small, R. K. Kalia, A. Nakano, and P. Vashishta, Comput. Phys. Commun. **192**, 91–96 (2015).

[21]A. M. N. Niklasson, Euro. Phys. J. B **94**(8), 164 (2021).

[22]A. Vaswani, N. Shazeer, N. Parmar, J. Uszkoreit, L. Jones, A. N. N. Gomez, L. Kaiser, and I. Polosukhin, in Advances in Neural Information Processing Systems (NIPS 2017), 2017, Vol. 30.

[23]A. Mishra, L. Chen, Z. Li, K. Nomura, A. Krishnamoorthy, S. Fukushima, S. C. Tiwari, R. K. Kalia, A. Nakano, R. Ramprasad, G. Sotzing, Y. Cao, and P. Vashishta, Comput. Mater. Sci. **228**, 112340 (2023).

[24]A. A. Deshmukh, C. Wu, O. Yassin, A. Mishra d, L. Chen, A. Alamri, Z. Li, J. Zhou, Z. Mutlu, M. Sotzing, P. Rajak, S. Shukla, J. Vellek, M. A. Baferani, M. Cakmak, P. Vashishta, R. Ramprasad, Y. Cao, and G. Sotzing, Energy Environ. Sci. **15**(3), 1307–1314 (2022).

[25]F. Shimojo, S. Fukushima, H. Kumazoe, M. Misawa, S. Ohmura, P. Rajak, K. Shimamura, L. Bassman, S. C. Tiwari, R. K. Kalia, A. Nakano, and P. Vashishta, SoftwareX **10**, 100307 (2019).

[26]P. E. Blochl, Phys. Rev. B **50**(24), 17953–17979 (1994).

[27]G. Kresse and J. Furthmuller, Phys. Rev. B **54**(16), 11169–11186 (1996).

[28]J. P. Perdew, K. Burke, and M. Ernzerhof, Phys. Rev. Lett. **77**(18), 3865–3868 (1996).

[29]S. Grimme, J. Comput. Chem. **27**(15), 1787–1799 (2006).

[30]A. Musaelian, S. Batzner, A. Johansson, L. Sun, C. J. Owen, M. Kornbluth, and B. Kozinsky, Nat. Commun. **14**(1), 579 (2023).

[31]H. Ibayashi, T. M. Razakh, L. Yang, T. Linker, M. Olguin, S. Hattori, Y. Luo, R. K. Kalia, A. Nakano, K. Nomura, and P. Vashishta, Proc ISC **13948**, 223–239 (2023).